



ALMA MATER STUDIORUM
UNIVERSITÀ DI BOLOGNA

DEPARTMENT OF INDUSTRIAL ENGINEERING

BACHELOR'S DEGREE IN MECHANICAL ENGINEERING

**DESIGN AND 3-D PRINTING
MANUFACTURING OF A POLYMERIC
HEAT SINK.**

Supervisor
Prof. Marco Lorenzini

Presented by
Lorenzo Cagnani

Co-Supervisor
Prof.ssa Francesca De
Crescenzo

March session 2025
Academic Year 2024/2025

Table of contents:

1. Introduction.....	3
1.1. Objective of the thesis.....	3
1.2. Structure of the work.....	3
2. Theoretical Background.....	4
2.1. Forced convection.....	4
2.2. Rectangular fin heat sinks.....	5
3. Heat sink design.....	6
3.1. Generated Data.....	6
3.2. Sizing and choice of the materials.....	7
3.3. Optimization and design challenges.....	10
4. Design and choice of the remaining components.....	11
4.1. Pump.....	11
4.2. Manifolds.....	12
5. Results Analysis.....	13
5.1. Simulation results.....	13
5.2. 3D models.....	14
6. Conclusions.....	15

1. Introduction

1.1. Objective of the thesis

The objective of this thesis is to develop a heat sink by additive manufacturing taking advantage of the material and process being particularly cheap and not employing metal or carbon-based materials. To achieve this goal, I have developed a physical-mathematical model to investigate the behaviour of different ranges of dimensions when designing the heat sink. By doing this, not only do I dramatically cut the time of computation, either by hand or by software, but I am also able to use values available in the traditional bibliography by simulating their trend using a code written in Matlab. By being easy to produce, standardized dimensions are only required for the pumps. Also, it is far easier to dispose of the heat sink since it is made of ABS plastic, which has a higher recyclability than standard materials used for heat sinks; and being made with additive manufacturing, the only production waste is the print supports. Additionally, subsequent studies will be able to devise new geometries taking advantage of the new possibilities unlocked by the use of a 3D printer. However, because of the low melting point to avoid reaching too high temperatures, the system runs on silicone oil instead of water and is generally limited to working with temperatures not above 150°C, even for the most resistant plastics. To close the loop, once its dimensions are defined, the collectors and the pump are chosen based on the requirements such as flow rate, fluid speed and viscosity.

1.2. Structure of the work

The first calculations were done by hand so as to directly obtain the dimensions in one go, however the efficiency was too low. Once figured out it was due to the plastic's low thermal conductivity, instead of determining the size, the key question became: which specific plastic should be used among the various types? Working on that I was able to maintain about 50% efficiency (instead of the starting 16%) while not needing to resort to carbon or metallic inclusion, making it more affordable and not needing elaborate types of printers. All of that is handled by a Matlab script which takes inputs like: required fin efficiency, desired thermal conductivity and overall dimensions; then the program starts running and outputs every data needed to build it with that set of parameters, like fluid speed and heat flux. After that the heat sink is drawn on SolidWorks so that it can be converted to a file for the 3D printer, during the printing process, thermocouples are embedded into the lower wall of the heat sink, to check the temperature profile along the channels y. They are inserted on the top of the channels, and they register the temperature of the surroundings where their junction is placed so it is important to ensure that; their two wires are not touching anywhere else, or the recorded data will be useless. To ensure accurate data collection, tests are conducted at a room temperature of 20°C, with the heat sink base maintained at 70°C using plate heaters. After it is ready it is connected to the collectors and their inlets are linked to the pump with tubes, once the environmental conditions are checked the oil is pumped into the system, everything is turned on and the proper measurements are made.

2. Theoretical Background

2.1. Forced Convection

When a fluid with a given velocity moves through a pipe we are in the case of forced convection. In this situation we use non-dimensional values that express different types of ratios in my system, like the Reynolds, Nusselt and Prandtl numbers:

$$Re = \frac{v \cdot D_h}{\nu} \quad (1)$$

$$Nu = \frac{h \cdot L}{k_f} \quad (2)$$

$$Pr = \frac{\nu}{\alpha} \quad (3)$$

The Reynolds number expresses inertial forces over viscous forces and is the indicator of the flow type between laminar, mixed and turbulent; under a Re of about 2300 we can be sure to be under the case of laminar flow. Since the project is small, maintaining a laminar flow regime is crucial. It means that the particles in the oil flow following straight lines parallels to the duct walls. The Nusselt number is the heat transferred by convection over the heat transferred by conduction; a high Nusselt number indicates a prevalence of convection heat transfer over conduction. Also, the number depends on the flow type, for laminar flow it ranges from about 1 to 10, that is what will be used. Prandtl number is the momentum diffusivity over thermal diffusivity; in our case because the oil has a high viscosity, we expect a number much larger than 1, it means that the heat transfer is far slower than the momentum transfer. Having laminar flow also enables us to calculate the lengths after which the fluid is fully developed, it is particularly significant because while not fully developed the characteristics of the inner wall of the pipe influence the proprieties of the fluid. Having a developed flow also means we can use an average value for velocity and a stable heat transfer convection coefficient, after the entry region the profiles turn from flat to parabolic, indicating the laminar flow as can be seen below:

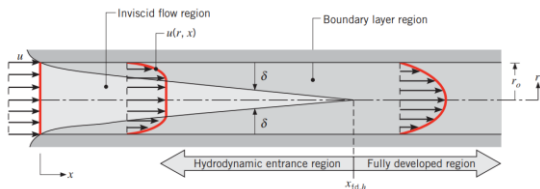


Figure 1: Laminar, hydrodynamic boundary layer development in a circular tube [1].

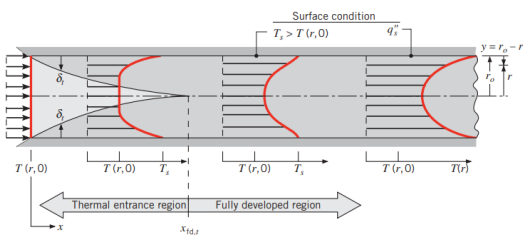


Figure 2: Thermal boundary layer development in a circular tube with a hot wall [1]

In our case the entry region is about 20% of the length of the duct, without this hypothesis the Nusselt relation is not precisely defined and becomes generically:

$$Nu_D = C \cdot Re^m \cdot Pr^n \quad (4)$$

$$x_{fd} \approx 0,05 \cdot Re_D \cdot D_h \quad (5)$$

Since $Pr > 1$ it means that the thermal entrance region is far longer than the hydrodynamic one, so it is reasonable to assume a fully developed velocity profile throughout the thermal entry region.

$$x_{fd} \approx 0,05 \cdot Re_D \cdot Pr \cdot D_h \quad (6)$$

2.2. Rectangular fin heat sinks

The theory at the base of fins is that for an extended surface, the direction of heat transfer from the boundaries is perpendicular to the principal direction of heat transfer in the solid. While it happens the sides of the fins are in contact with the moving fluid taking advantage of the convection heat transfer, since $Nu > 1$ it is far better and efficient than conduction. So, by having multiple fins we try to output more and more heat flow while also leaving the overall efficiency high. Depending on the width of the channel in literature there two main cases of study, what differentiates them is the way the flow develops:

- Small-spaced fins

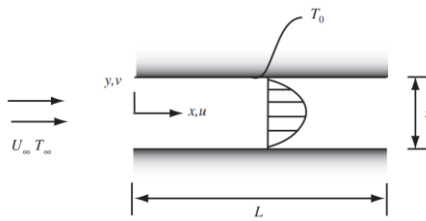


Figure 3: Fully developed flow for the small spacing channel [2].

One unique boundary layer is formed, analog to the one seen in the fully developed flow in a duct. The heat transfer proportion is:

$$q_f \propto z^2 \quad (7)$$

- Large-spacing fins

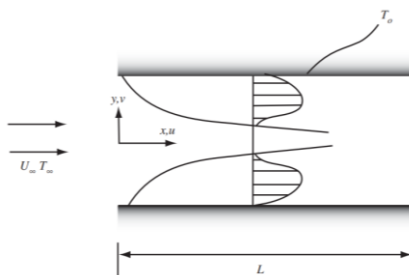


Figure 4: Isolated flows over the upper and lower plates for a large spacing channel [2].

The passage is large enough to simulate the condition of isothermal plates, profile splits in two ones for each wall. The heat transfer proportion is:

$$q_f \propto z^{\frac{2}{3}} \quad (8)$$

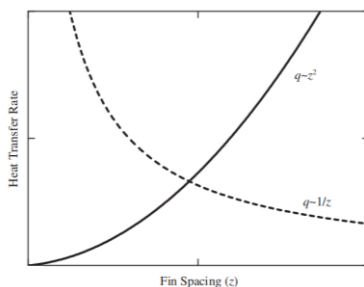


Figure 5: Optimal fin spacing (z) for the maximum heat transfer rate by natural convection between two vertical isothermal plates [2].

By combining the two different cases, similar to the natural convection plot, we can find the optimum fin spacing to maximize heat transfer as:

$$\frac{z_{opt}}{L} = 3.24 \cdot Re^{-\frac{1}{2}} \cdot Pr^{-\frac{1}{4}} \quad (9)$$

Having previously defined the Re and Pr numbers, we can now determine the optimum fin spacing; or in our case we will start from the last equation to find the required Re to satisfy the required characteristic.

3. Heat sink design

3.1. Generated Data

As said previously, the Nusselt number (2) is only determined for limited types of geometries. However, using the Matlab Simulink add-on, we can use these values to plot a continuous graph in a determined interval. To do it the fitype function is used, the set of results is used to plot the single points, then depending on the grade of the polynomial a generic fit is generated to represent a possible tendency. The approximation chosen was of a quadratic polynomial; since using polynomials of higher degree yields a relative maximum, while the graph must be monotonically increasing. When the function is run a Vandermonde matrix named X to represent the linear system is created, which is a matrix where its elements are elevated to a determined power and then follow a geometric progression on the rows or columns. Then it's combined with the vector B of known coefficients and the ϵ vector of residual error, together they represent the vector of observed Nu values.

Generic quadratic equation:

$$y = ax^2 + bx + c \quad (10)$$

Matrix representation equation:

$$Y = XB + \epsilon \quad (11)$$

After that the least squares method is used to evaluate the errors of between the esteems and the observed data; once the most precise vector B is found the gradient of the equation is set to 0 to find the normal equation. By solving it for B we have the values to use in the generic quadratic equation and to plot the results:

Least square method:

$$\min ||Y - XB||^2 \quad (12)$$

Normal equation:

$$(X^T X)B = X^T Y \quad (13)$$

Cross Section	$\frac{b}{a}$	$Nu_{D_h} = \frac{hD_h}{k}$		fRe_{D_h}
		(Uniform q_w')	(Uniform T_w)	
	—	4.36	3.66	64
	1.0	3.61	2.98	57
	1.43	3.73	3.08	59
	2.0	4.12	3.39	62
	3.0	4.79	3.96	69
	4.0	5.33	4.44	73
	8.0	6.49	5.60	82
	∞	8.23	7.54	96
	∞	5.39	4.86	96
	—	3.11	2.49	53

Adapted from W. M. Kays and M. E. Crawford, *Convective Heat and Mass Transfer*, 3rd ed. McGraw-Hill, New York, 1993.

Figure 6: Nusselt numbers and friction factors for fully developed laminar flow in tubes of differing cross section [1].

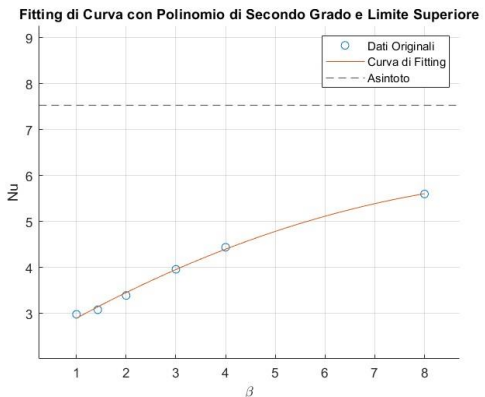


Figure 7: Nusselt number function in tubes of differing cross section [3].

With this new data we can arbitrarily choose a value of beta (the ratio between the base and the height of the channel) if it's contained between 1 and 8. Since the values are generated a part of the program makes sure to use experimental results when possible, because in order to define a clear polynomials the Nusselt numbers leave a margin of error in the prediction.

Since we have an adiabatic tip the efficiency equation uses the hyperbolic tangent (14), a transcendental function; that is the result of solving the Fourier equation, which since it's a differential equation has its solution in the form of e^x . All of it means that we cannot normally isolate just one of the parameters, in our case the fin conductivity, which is contained in m. The only option left is to make the function only dependent on one variable,

this way we bypass having an infinite number of solutions from the product of the two terms, that is why the parameter C is defined as

$$\eta = \frac{\tanh(m \cdot b)}{m \cdot b} \quad (14)$$

$$C = m \cdot b \quad (15)$$

Starting from a generic value of C a numerical method is used to find the precise number needed for a target single fin efficiency performance. It works based on proportional updates: with the starting C an η is calculated and the error between the desired η is evaluated; if the error is lesser than the set tolerance it means the current C is the correct one. If it is higher C is updated based on the ratio between the η and the whole process is repeated, this way no matter which starting point is chosen, it makes sure to have a finite value as a result of convergence; if the efficiency is between 1 and 99. In the possibility of it not reaching a finite value, after a set number of interactions, the script will stop displaying an error message.

```
% Calcolo di C
while iterazioni<iterazioni_massime
eta_attuale=tanh(C)/(C);
errore=abs(eta_attuale-eta);
if errore<tolleranza
break;
end
C=C*(eta_attuale/eta);
iterazioni=iterazioni+1;
end
if iterazioni==iterazioni_massime
error('Convergenza non raggiunta: controllare i parametri di input');
end
```

Appendix A: Matlab Code

3.2. Sizing and choice of the material

Since the polynomial is continuous between 1 and 8 a function is used to simulate a continuous range of different measures: *linspace*. Once the number of subdivisions is set the system creates a vector of n evenly spaced points in the interval; by setting it small enough the result is the coverage of all possible sizes. That is because with a number based on the printer the steps represent the minimum print resolution, so from one possibility to another you cannot physically have a different measure since the extruder cannot move less than that distance. By making it the same size of the β array I can reverse the relation because β and b are chosen in advance:

$$\beta = \frac{z_{opt}}{b} \quad (16)$$

$$D_h = \frac{2 \cdot z_{opt} \cdot b}{z_{opt} + b} \quad (17)$$

Doing that gives me a $n \times n$ matrix of possible z values, from this point onwards all the data calculated are in the form of matrix, that means the sequent results can be evaluated in a more complex and complete way. Since m is defined as:

$$m = \sqrt{\frac{h \cdot P}{k_s \cdot A_s}} \quad (18)$$

$$C^2 = \left(\frac{h \cdot P}{k_s \cdot A_s} \right) \cdot b^2 \quad (19)$$

Combining the previous equations, after simplifying the ratio between the fin perimeter P and the fin area A_s and calculating the convection coefficient h based on the Nusselt equation (2), yields the result of:

$$k_s = \frac{(2 \cdot h \cdot b^2) \cdot \left(1 + \frac{t}{L}\right)}{t \cdot C^2} \quad (20)$$

Before being able to make any consideration on the results, all the remaining parameters must be evaluated. Among these, the fluid velocity and the value of Re needed for the optimal z sizes, and most important the overall efficiency and heat flux for performance reasons:

$$\eta_0 = 1 - \frac{nA_f}{A_t} (1 - \eta_f) \quad (21)$$

$$q_{total} = \frac{\theta_b}{R_{t,o}} = \theta_b \eta_0 h A_t \quad (22)$$

For the oil used its chemical formula is $C_6H_{12}OSi_2$; for its density and viscosity a set of previous studies was used which tests were also done at $20^\circ C$. It's slightly less dense than water with a value of $930 \frac{kg}{m^3}$, however its dynamic viscosity is $11mPas$ which is about 10 times higher than water, this limits the convection. However, it is commercially available, chemically stable and does not evaporate under test conditions, which makes it an excellent substitute for water. [4]

For the printer's filament ABS P430 was used, alongside a series of other plastics it is one of the better heat conductors and one of the most commercially used. Since 3D printing is an anisotropic process, it would be incorrect to assume just one unique value of conductivity for all three-dimensional axes. Previous studies have been made to characterize 3D printed cubic samples; their values range from 0,1 to $0,5 \frac{W}{mK}$, making them more like heat insulators than conductors. That combined with the high viscosity of the oil are the reasons why this model cannot reach high performance, still by using fluids and materials with a higher order of magnitude of conductivity the heat sink can become the main and only source of heat dissipation.

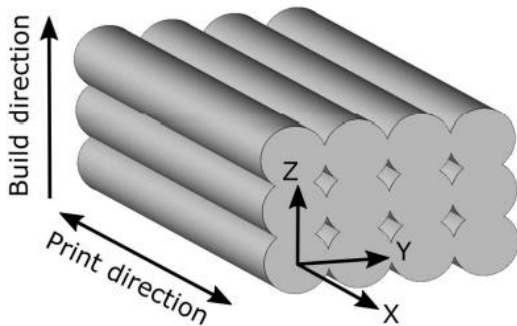


Figure 8: Illustration of print and build directions of 3D printed samples [5].

Material	Density, g/cm^3	K_x , W/m-K	K_y , W/m-K	K_z , W/m-K	C_p , kJ/kg-K
PLA_TW	1.227 ± 0.002	0.229	0.23	0.229	1.25 ± 0.08
PLA Red	1.203 ± 0.007	0.247	0.189	0.206	1.26 ± 0.04
PLA LAVA	1.246 ± 0.000	0.23	0.231	0.228	1.24 ± 0.06
PLA Con- ductive	1.212 ± 0.002	0.434	0.348	0.309	1.29 ± 0.13
PET-G	1.276 ± 0.003	0.248	0.23	0.246	1.12 ± 0.06
ABS	1.124 ± 0.001	0.228	0.223	0.227	1.26 ± 0.08
CPE	1.273 ± 0.002	0.271	0.252	0.235	1.09 ± 0.08
PC	1.191 ± 0.001	0.256	0.258	0.256	1.26 ± 0.11
PP	0.813 ± 0.016	0.286	0.181	0.178	1.96 ± 0.19
TPU95A	1.033 ± 0.019	0.246	0.253	0.187	1.78 ± 0.22
PA	1.103 ± 0.006	0.337	0.362	0.304	1.89 ± 0.09
PEKK	1.199 ± 0.003	0.242	0.235	0.241	1.06 ± 0.07
PEI	1.173 ± 0.001	0.269	0.191	0.183	1.12 ± 0.10

Table 1: Physical proprieties of investigated samples [5]

When choosing the material, other than the conductivity and commercial availability, also its deformability comes into play. Each filament has its own softening point, as of standard definition ISO 306, when a needle with a cross section of 1 mm^2 penetrates the material for 1 mm depth at a given temperature that is called softening temperature. For plastic filaments that value ranges from 50 to 200°C and it shows no direct correlation between its corresponding λ . According to the fin theory the heat will flow through the printing direction z , nonetheless if one of the coefficients offers outstanding performances all that is needed to do is to rotate the heat sink to the desired orientation in the slicing software.

[6]

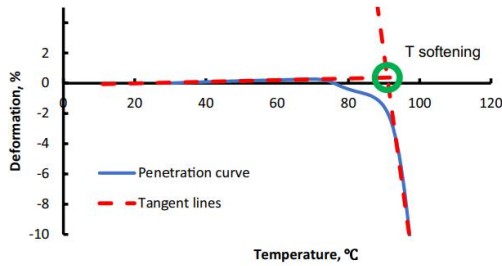


Fig. 3 Determination of softening temperature T_s for ABS sample by a TMA penetration test

Figure 9: Determination of softening temperature T_s for ABS sample by a TMA penetration test [5].

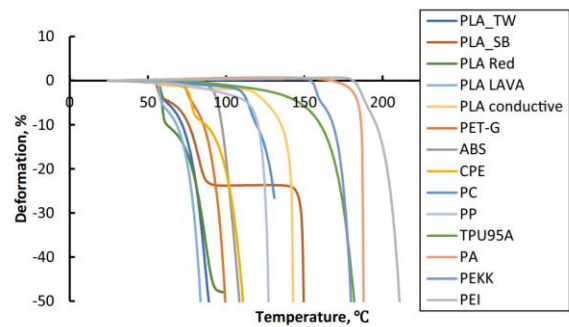


Figure 10: TMA curves of the deformation as a function of temperature for penetration of tested samples [5].

As presented by the same study there is also a difference based on how much time the filament had been stored; it has been observed that for these materials just a two-week period can slightly alter the shape of their heating circle. That is not a problem for the application itself since the system is operating under deformation temperature; instead, it is a concern for the print phase. If the spool had been in storage for a long time without it being reconditioned the risk is to calibrate the hotend wrong and not give it the sufficient temperature to properly melt. When that is the case, the result is a misplacement of the crystalline structure, leading to a different conduction coefficient than the one obtained during standardized testing.

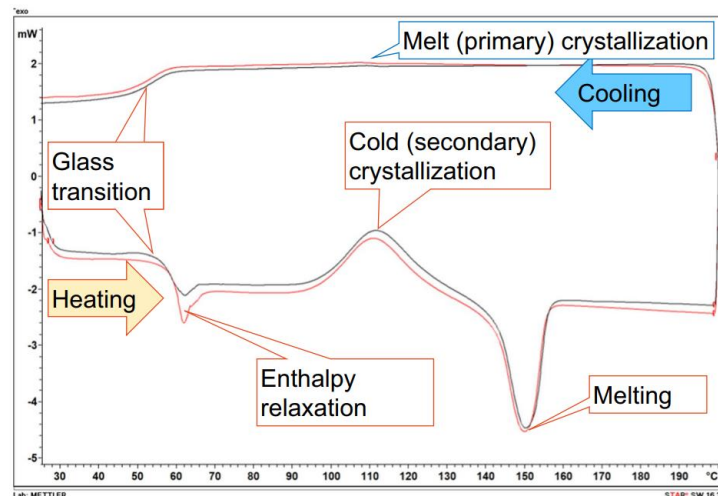


Figure 11: Heat flow (mW) vs temperature ($^\circ\text{C}$) for 3D printed specimens in DSC test: Fresh sample (black line) with storage time less than 1 day; old sample (red line) with storage time more than 16 days [5].

3.3. Optimization and design challenges

Each of the data represented by a matrix is expressed as a surface in a 3D graph, this way by slicing it when its trend is not uniform the outcome are multiple points with the same desired characteristics. Since the goal of this thesis is maximizing heat dissipation, heat flux q_f is used as the main discriminant. For each profile that matches the desired coefficient a comparison is run to determine which was the one with the highest heat transfer. However, this is not the only problem to take into consideration: because this solution is thought for domestic and academic usage the average bed size for the printer hardly surpasses 250mm. So, it is possible that the optimal dimensions involve exceeding the bed limits; when that is the case the program automatically discards the first solution and moves on to examine the second best one and so on. This process does not affect calculations because its width is not used in any of the previous equations, resulting in a rectangular-shaped heat sink; its side walls thickness is kept half that of the fin base. Analogous to this filter another one is used for the fluid velocity: given that the possible channel width and height are considered when the sizes for both are at their minimum, so it is for their hydraulic diameter. The outcome is an extremely rapid increase in the speed needed to achieve optimal results, by about two orders of magnitude, meaning that the flow rate and pump needed are completely out of scale. The solution is the same adopted for the width problem: setting a filter that excludes data sets with a too high required speed. On the other side another filter is needed to exclude situations where the speed values were below the $\frac{cm}{s}$, because it is too low to properly manage. In the end even all the Re numbers are not all usable, since the velocity tends to spike with smaller ducts in that portion Re will be above 2300, which is about the limit when laminar flow starts being mixed flow, making some of the equations used not valid. Also, the manifolds studies are done for $Re < 600$, with the best results at 200. That is why only cases where Re is less than 2000 are considered.

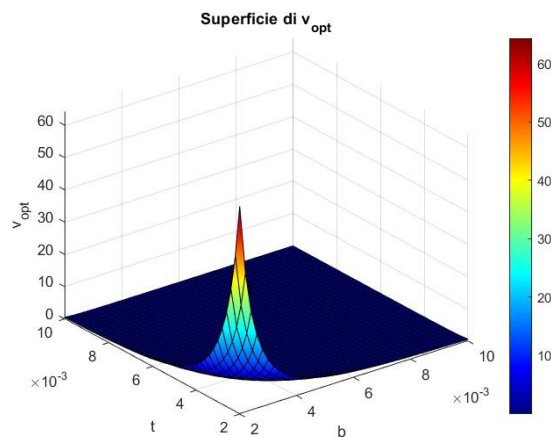


Figure 12: Fluid speed distribution in relation to fin dimension [3].

The last problem regarding the calculation are the matrix operations themselves, considering that in various calculations multiplications or divisions are between matrix and vector they cannot be done with the rules of regular algebra since their sizes sometimes does not match. To solve this issue Matlab is equipped with elementwise multiplication and division; it means that the result is obtained by calculating every element of the matrix with every element of the array. Since matrix operation is not commutative the results will have a small percentage of error, nonetheless the inaccuracy is so little that it does not alter the overall performance.

4. Design and choice of the remaining components

4.1. Pump

What the data and the results tell is that we need a pump that can deal with a really viscous fluid, can output very small flow rate and does not care about giving elevated pressure or prevalence to the fluid. It should be also easy to control the fluid speed to stick as much as possible to the Matlab calculations. Because of the high viscosity of the oil a traditional centrifugal pump cannot bear the frictional dissipations, so a volumetric one is the right way to proceed; the choice falls under four different categories:

- Gear pumps
- Lobe pumps
- Diaphragm pumps
- Peristaltic pumps

Going down that path we can exclude gear pumps because they are more oriented for high pressure application and peristaltic pumps because they are difficult to regulate and for a higher flow rate. For diaphragm pumps due to the alternating movement of the diaphragm, the flow is not constant and may require a pulsation dampener. The final decision is for the lobe pump, particularly the motorized BE125-F1 produced by O.M.A.C. S.r.l.. It is made to operate with fluids ranging from 1 to 500 cP (one centipoise equals one $mPa \cdot s$), it can reach up to $18 \frac{l}{min}$ as flow rate and is equipped with an IP65 inverter. All the operational values are obtained from the pump catalogue on their webpage.

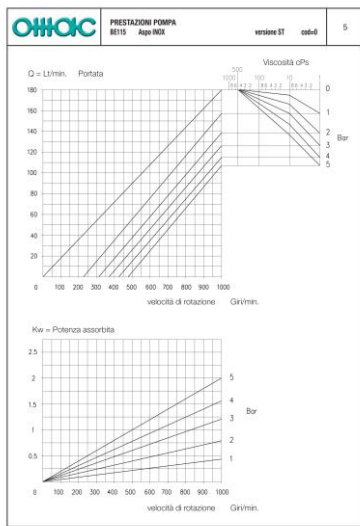


Figure 13: BE125 lobe pump characteristic curves [7].



Figure 14: BE125 lobe pump general technical data [7].

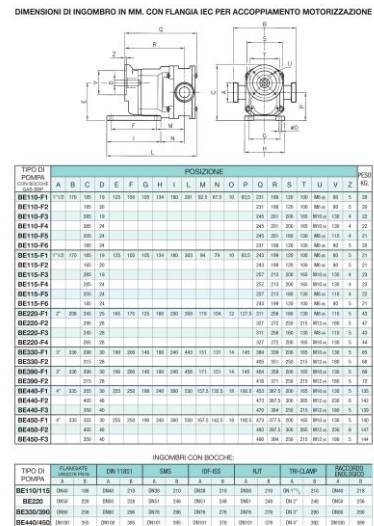


Figure 15: BE125 lobe pump overall dimensions [7].

Among all the BE to choose from the 125 is the second smallest pump they sell; it was picked instead of the 110 because even if it can reach a higher flow rate that is not needed it operates from 1 to 5 bars, instead of 1 to 7 of the 110, making it cheaper. This way the pressure drop will be less severe and if it is needed it can suit higher flow rates. As for actual performance, it is estimated for it to function at around 60 rpm and its power consumption to be around 50 W. Since our oil dynamic viscosity is just 1.1 cP the pressure drop is negligible.

4.2. Manifolds

The main issue when designing a manifold, is to obtain a uniform flow throughout all of the channels. The standard baseline configuration, even at Re numbers below 600, shows a normal distribution of the fluid velocity; leaving the most external channels with an insufficient flowrate to disperse enough heat. Recent studies have been made regarding the use of baffles, followed by testing with parametric and topological models. Given that the topological models use very complicated geometries for the baffles, for this configuration parametric baffles were chosen. The design requires baffles to increase in size following a logarithmic shape curve, since the results of the precise measures are obtained with extensive testing and precise geometries a very generous approximation is made to adapt the results. To achieve it like the Nu number, graph a fitype of an exponential function is employed.

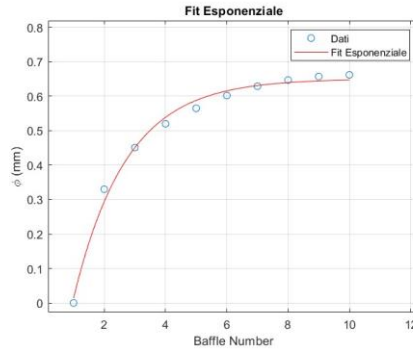


Figure 16: Exponential fit of baffles diameters [3].

By having half the number of inlets, the generated curve is divided to suit the difference. Since the liquid speed arranges in a normal distribution by adding an inverted normal distribution through the baffles it levels out the differences leaving an almost uniform distribution. In the study it is noted that for manufacturing reasons the baffles are adapted to an elliptical shape instead of a circular one using coefficients found after extensive tries; by printing them there is no issue with using the original layout. The baffles force part of the fluid to go back into the manifold, the increase in size helps to equally distribute the flow. For all the other measures used, they are scaled proportionally from the original design,

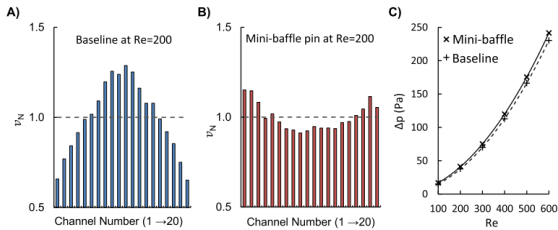


Figure 17: Experimental normalized channel flow rates (v_N) for A) PDMS baseline and B) mini-baffle pin configurations. C) Pressure drops for baseline and mini-baffle pin from the 3D numerical model [8].

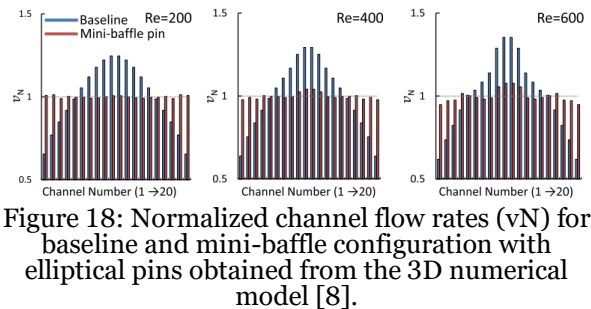


Figure 18: Normalized channel flow rates (v_N) for baseline and mini-baffle configuration with elliptical pins obtained from the 3D numerical model [8].

i	1	2	3	4	5
ϕ	0	0.478	0.604	0.637	0.662

Table 2: Baffles dimensions in mm for a heat sink with 10 channels.

5. Result Analysis

5.1. Simulation results

The results from the Matlab model appear promising. By imposing a single fin efficiency of 50% the simulation yields an overall efficiency of 82.2% and a comprehensive heat flow of 0.1 kW. Also, the hydrodynamic development length is just under 6 cm out of the total 20, assuring compatibility with the equations used.

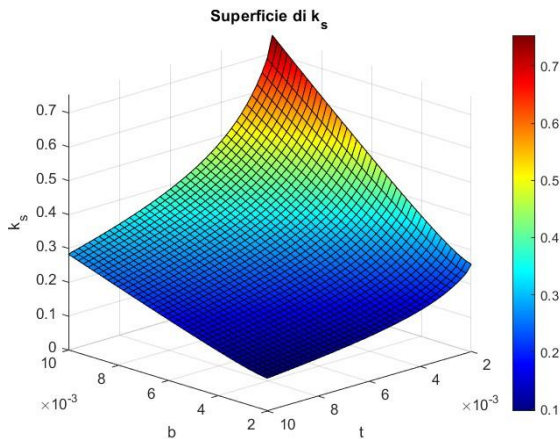


Figure 19: Build direction conduction ABS coefficient distribution in relation to fin dimension [3].

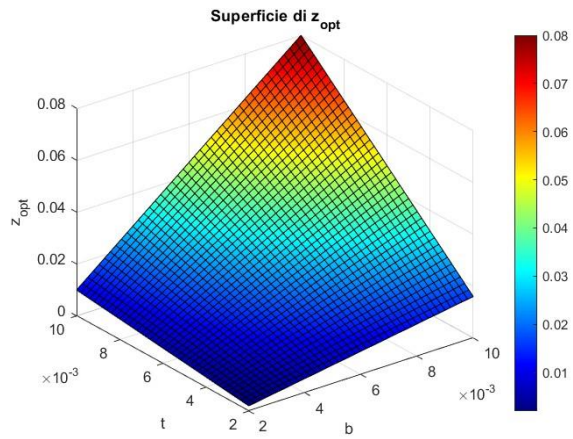


Figure 20: Channel width distribution in relation to fin dimension [3].

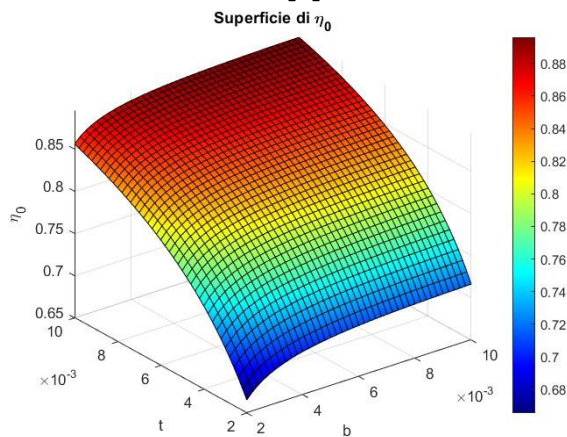


Figure 21: Overhaul heat sink efficiency distribution in relation to fin dimension [3].

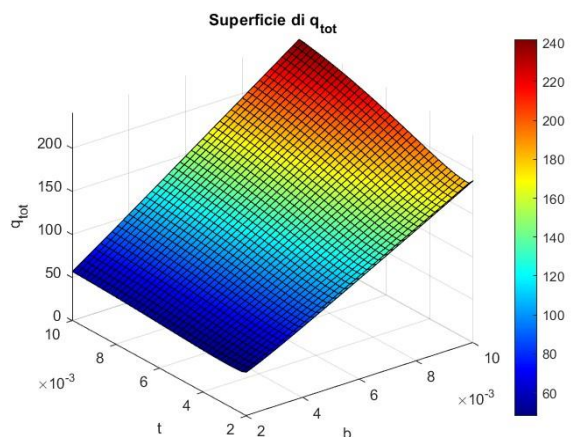


Figure 22: Overhaul heat flow distribution in relation to fin dimension [3].

The data stored in matrix are represented with the *surf* function, with it a color bar can be set to better visualize the surface tendency. As expected, the most outstanding results come from the maximum dimensions of fin and channel height and thickness; nonetheless the required conductivity tends to its highest point for slim and elongated fins. All these results are theoretically possible, the best fins come from a slender shape, explaining the distribution of λ ; at the same time, having an elevated stream of oil increase the heat dissipated by convection, boosting the global performance of the heat sink

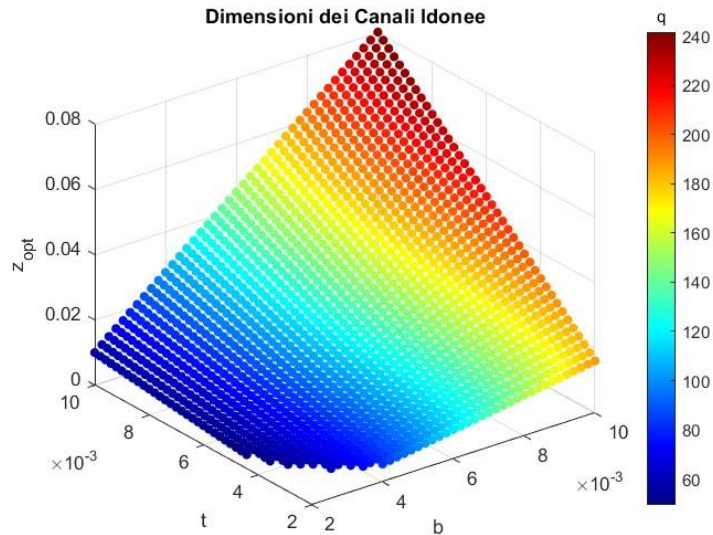


Figure 23: Suitable overhaul heat flow distribution in relation to heat sink channel and fin dimensions [3].

Combining all the previous results in one graph can lead to a general understanding of the heat exchange in heat sinks. Instead of the *surf* function, which requires a square matrix to operate, the *scatter* function is used, that is because of the various criteria explained in paragraph 3.3. Having to check and differentiate the matrixes is far more difficult than unwinding them as single arrays, once done the unfeasible positions are discarded, as can be seen in the corner of the graph. Its three axes represent all the dimensions of fins and channels, along with the color bar depicting the heat flow, this way all the data needed for an initial performance and size analysis are displayed on the screen.

5.2. 3D models

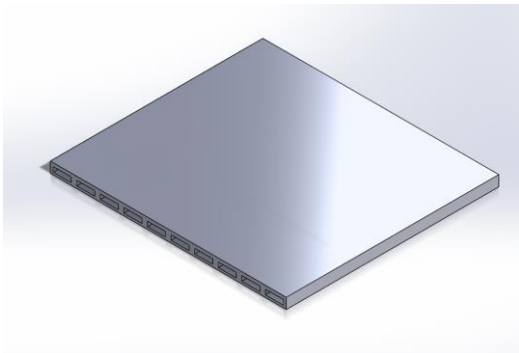


Figure 24: Theorized heat sink [9].

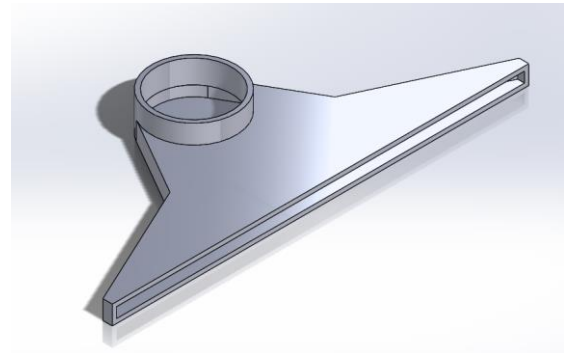


Figure 25: Approximated manifold [9].

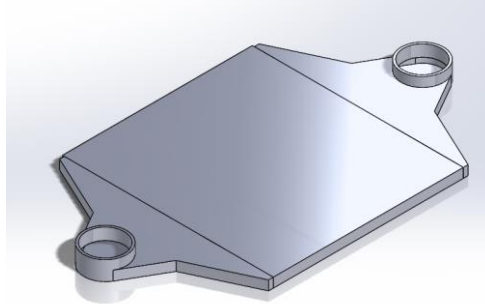


Figure 26: Prototype assembly [9].

6. Conclusions

The approach taken has demonstrated that additive manufacturing offers an interesting alternative to traditional heat sinks, especially in low-temperature applications and for educational or research purposes. However, the system's efficiency could be further improved by using polymer materials with higher thermal conductivity or through optimizations of the internal geometry to enhance heat transfer by convection. As previously theorized and now confirmed, the use of non-standardized geometry for the configuration of the heat sink offers new possibilities and perspectives for customizable projects; however, it comes with its own set of unique challenges. Even though most volumetric pumps can supply with the right flow rate and easily move highly viscous fluids, managing to precisely control and distribute evenly the fluid velocity in all the cavities can be a particularly difficult task. This specific problem can be solved by extensive research and standardized dimensions for parametric designed manifolds or models for topological manifold; once this issue is addressed it becomes particularly easy to model an entire system of cooling. Nonetheless, as it can seem easy to scale the idea using significantly better materials and larger sizes, it is reminded that all the calculations are done under the hypothesis of laminar flow, so the biggest limitation of the project is the unavailability for applications at high speeds or uncontrollable environments. For the same reason, because of the delicate geometry of the manifolds, there is the chance that the pump outlet is not of the same dimensions of the manifold inlet. So, at the same time, it is important not to use a too steep divergent or convergent tube because it can disrupt the laminar flow by creating vortex shedding or flow separation; and not to be too long because of the distribution head losses. As for its replicability the only thing to be aware of is the effect of time on plastic spools that are stored for long periods as they cannot rearrange in an extremely precise structure. In conclusion, while the approach shows significant potential for innovation in heat sink design, further research and development are necessary to fully optimize the system for broader applications. With continued improvements in material science and design techniques, additive manufacturing could revolutionize the way we approach thermal management in various fields.

Index of figures

Figure 1: Laminar, hydrodynamic boundary layer development in a circular tube [1].....	4
Figure 2: Thermal boundary layer development in a circular tube with a hot wall [1].....	4
Figure 3: Fully developed flow for the small spacing channel [2].....	5
Figure 4: Isolated flows over the upper and lower plates for a large spacing channel [2]....	5
Figure 5: Optimal fin spacing (z) for the maximum heat transfer rate by natural convection between two vertical isothermal plates [2].....	5
Figure 6: Nusselt numbers and friction factors for fully developed laminar flow in tubes of differing cross-section [1].....	6
Figure 7: Nusselt number function in tubes of differing cross-section.....	6
Figure 8: Illustration of print and build directions of 3D printed samples [5].....	8
Figure 9: Determination of softening temperature for ABS sample by a TMA penetration test [5].....	9
Figure 10: TMA curves of the deformation as a function of temperature for penetration of tested samples [5].....	9
Figure 11: Heat flow (mW) vs temperature (°C) for 3D printed specimens in DSC test: Fresh sample (black line) with storage time less than 1 day; old sample (red line) with storage time more than 16 days [5].....	9
Figure 12: Fluid speed distribution in relation to fin dimension [3].....	10
Figure 13: BE125 lobe pump characteristic curves [7].....	11
Figure 14: BE125 lobe pump general technical data [7].....	11
Figure 15: BE125 lobe pump overall dimensions [7].....	11
Figure 16: Exponential fit of baffles diameters [8].....	12
Figure 17: Experimental normalized channel flow rates (vN) for A) PDMS baseline and B) mini-baffle pin configurations. C) Pressure drops for baseline and mini-baffle pin from the 3D numerical model [8].....	12
Figure 18: Normalized channel flow rates (vN) for baseline and mini-baffle configuration with elliptical pins obtained from the 3D numerical model [8].....	12
Figure 19: Build direction conduction ABS coefficient distribution in relation to fin dimension [3].....	13
Figure 20: Channel width distribution in relation to fin dimension [3].....	13
Figure 21: Overall heat sink efficiency distribution in relation to fin dimension [3].....	13
Figure 22: Overall heat flow distribution in relation to fin dimension [3].....	13
Figure 23: Suitable overall heat flow distribution in relation to heat sink channel and fin dimensions [3].....	14
Figure 24: Theorized heat sink [9].....	14
Figure 25: Approximated manifold [9].....	14
Figure 26: Prototype assembly [9].....	14

Index of tables

Table 1: Physical properties of investigated samples [5].....	8
Table 2: Baffles dimensions in mm for a heat sink with 10 channels [8].....	12

*Un ringraziamento speciale a tutte le persone
che mi sono state vicine durante questo percorso*